Topological properties of an SU(3) gauge system near the critical temperature on an anisotropic lattice

T. Hashimoto
Department of Physics, Heidelberg University, Philosophenweg 16, D-6900 Heidelberg, Federal Republic of Germany

S. Hioki
Department of Applied Mathematics, Faculty of Engineering Science, Osaka University, Toyonaka, Osaka 560, Japan

K. Hirose
Teikoku Women's University, Moriguchi, Osaka 570, Japan

T. Kanki
Faculty of Science and Technology, Kinki University, Higashi-Osaka, Osaka 577, Japan

A. Kawazoe
Department of Applied Mathematics, Faculty of Engineering Science, Osaka University, Toyonaka, Osaka 560, Japan

M. Masujima
Fundamental Research Laboratory, NEC Corporation, Miyamaeku, Kawasaki, Kanagawa 213, Japan

O. Miyamura and Y. Osada
Department of Applied Mathematics, Faculty of Engineering Science, Osaka University, Toyonaka, Osaka 560, Japan
(Received 16 January 1990)

Topological quantities on an anisotropic SU(3) lattice around the critical temperature are studied. The distribution of instantons has been investigated through semilocal measurements of topological charge and magnetic and electric actions in the framework of a cooling method. The suppression of the topological susceptibility χ_t in a deconfining phase, seen on isotropic lattices, is found also on the anisotropic lattice. The instanton density is also suppressed above T_c. In addition to the instantons, other topological configurations are found and studied. Among those with no instantons, one class shows a vanishing topological charge density and metastable plateau of magnetic action in the cooling. Analyses of the magnetic charge, flux, and zero mode of a three-dimensional staggered fermionic operator indicate that such configurations have a nontrivial structure of magnetic flux and monopoles of the SU(3) gauge system.

I. INTRODUCTION

An investigation of the topological nature of a gauge field around the critical temperature of the deconfining transition seems useful in understanding the mechanism of confinement and chiral structure.[1,2] It is well known that instantons have a close relationship with the axial U(1) anomaly.[3] And its anomaly restoration at finite temperature is expressed by the suppression of instantons. As for magnetic monopoles, their role in non-Abelian gauge field theory has been discussed from different points of view. In the confinement phase, monopole condensation is expected to induce the dual Meissner effect.[4] Also in the deconfinement phase, the generation of a magnetic mass of gluons and screening of triality by monopoles have been discussed.[5]

These problems have been studied on isotropic lattices by several different methods.[6,7] Recent investigations of the instanton by isotropic lattices have shown a suppression of the topological susceptibility in the deconfinement phase.[7] A suppression of the monopole above the critical temperature has also been reported,[8,9] while a static monopole configuration has been observed more clearly in the deconfining phase.[10] They supply increasing evidence for the idea that changes of a topological nature are a dynamical issue connected with the deconfining and chiral transitions.

In this paper, we report the results of a topological study on an anisotropic lattice. As is well known, there are several different ways to simulate a finite-temperature system. Instead of the usual way of reducing the number of lattice sites in a temporal direction (isotropic lattice), we use a contracted lattice unit in a temporal direction (anisotropic lattice).[11] A motivation of the anisotropic lattice is to keep the sensitivity in the temporal direction even at high temperatures. On an isotropic lattice, the number of sites in the time direction is reduced to a very small number at high temperatures, and we then have insufficient degrees of freedom in the time direction to describe field configurations with good accuracy. Here, we will present the results of the topological susceptibility, instanton density, and measurements of the magnetic

charge and three-dimensional fermionic zero mode for a class of magnetic configurations on an anisotropic SU(3) lattice.

Recently, the anisotropic lattice has been investigated by Burgers, Karsch, Nakamura, and Stamatescu.[12] The lattice action is given as

$$S=\sum_n S(n)$$
$$=\beta\sum_n\left[\sum_{i<j}\frac{1-P_{ij}(n)}{\gamma}+\sum_{i\neq 0}[1-P_{0i}(n)]\gamma\right], \quad (1)$$

where β is the lattice coupling constant, the $P_{ij}(n)$ and $P_{0i}(n)$ are, respectively, the space-space and space-time plaquettes at site n. The parameter γ represents the lattice anisotropy. In the naive continuum limit we expect $\gamma=a_s/a_t$. However, it is subject to renormalization and we set $\gamma\eta=a_s/a_t$. In Ref. 12, η is then determined through the measurements of the lattice observables, such as Wilson loops. It was found that $\eta=1.31$ for an 8^4 lattice with $\gamma=2$. It was also confirmed that η has no β dependence at least over the range $5.65\leq\beta\leq 5.75$, where the critical coupling for the deconfinement phase transition was given as $\beta_c\simeq 5.67$.

The present paper is organized as follows. In Sec. II, the cooling method in the present analyses and data sampling are described. In Sec. III distributions of the topological charge and instanton below and above the critical point are presented. In Sec. IV we report analyses of the magnetic field, charge, and eigenvalues of a three-dimensional fermionic operator for a class of magnetic configurations. The last section is devoted to a summary and discussions.

II. SAMPLING AND COOLING METHOD

Topology is the long-range property of gauge field theory. In order to extract the topological nature of thermalized configurations, we use the so-called cooling method.[6] We perform the following iterations in the cooling stage, i.e., iterations by a classical equation of motion in fictitious time:[13]

$$U_\mu^{\text{new}}(n)=\exp[iX(n)]U_\mu^{\text{old}}(n) \quad (2)$$

and

$$X(n)=i(\delta\tau)t^a\text{tr}\left[t^aU_\mu(n)\frac{\delta S}{\delta U_\mu(n)}\right], \quad (3)$$

where $U_\mu(n)$ is a SU(3) link matrix and t^a are the group generators. The "step" parameter $\delta\tau$ of fictitious time adjusts the speed to the underlying classical configurations. (Larger $\delta\tau$ gives more acceleration but too large a value leads to fast decay of an instanton. We take $\delta\tau=0.04$.)

Different measurements are performed in the normal updating stage and the cooling stage. In the normal updating stage, the action and the Polyakov line are measured. The latter is used to distinguish the configuration to be cooled whether it is in the confining or deconfining phase. In the cooling stage, we have monitored the topological charge according to the formula[7]

$$Q=\sum_n\rho_Q(n), \quad (4)$$

$$\rho_Q(n)=\frac{1}{32\pi^2}\epsilon_{\mu\nu\rho\sigma}\text{tr}[P_{\mu\nu}(n)P_{\rho\sigma}(n)]. \quad (5)$$

In addition to the total topological charge, we also measure the quantity

$$I_Q=\sum_n|\rho_Q(n)| \quad (6)$$

and the normalized action $\tilde{S}$,

$$\tilde{S}=S/(4\pi\beta/3), \quad (7)$$

and space-space and space-time actions which convey information about the total number of instantons and anti-instantons. Furthermore, to obtain the semilocal distributions, we divide each direction into two sectors (0 and 1) and we measure these quantities in the 16 sublattices of size 4^4. [See Figs. 2(b) and 2(d).]

For assignment of multi-instanton configurations, I_Q and Q in the sublattices are quite helpful in identifying the existence of an instanton–anti-instanton pair. This pair gives no contribution to Q and their identification through $\tilde{S}$ is usually very difficult because of the slow convergence of $\tilde{S}$ along the cooling sweeps. With a rather high probability, such a pair can annihilate or decay before the convergence of $\tilde{S}$. In most configurations with a large instanton density, decays of instantons during the cooling sweeps can happen at a very early stage (80–150 sweeps). In this situation, we required a stabilization of I_Q and a localization of the topological charge over sublattices for the criterion for a multiinstanton configuration.

To check the reproducibility of the cooling method, we performed the cooling from the same configuration in the following different way. Cool by the classical equation of motion [Eq. (2)] with different time steps, and cool from different four-dimensional directions, and apply heat-bath cooling. All indicate the same topological result except the speed of convergence. We will come back to this point in Sec. IV.

In some cases, we add weak Gaussian random noise to the right-hand side of Eq. (3) in order to see the stability of the configuration against small perturbation. The topology is found to be unaffected by these short-range effects as expected.

In investigating the topological nature of the Monte Carlo–generated configurations, we must be careful of sequential correlation, and sample independent vacua. Then we define the topological correction length ξ from $\langle Q_kQ_{k+i}\rangle/\langle Q_k^2\rangle\propto\exp(-i/\xi)$ (Q_k is the topological charge at kth Monte Carlo sweeps and $\langle\ \rangle$ means the k average). Then we find $\xi=10$–20 in our 8^4, $\gamma=2$ SU(3) pseudo-heat-bath-generated configurations at $\beta=5.64$–5.70. Taking into account these facts, we prepare well thermalized SU(3) vacua and 100 pseudo-heat-bath updates have been made before the next sampling. Furthermore, the generations have been restarted for each five samplings. From this manipulation, we can avoid the topological correlation and get independent configurations.

III. TOPOLOGICAL CHARGE AND INSTANTON DENSITY

A. Cooling analyses of configurations

About 400 vacuum configurations each for the values $\beta=5.62$, 5.64, 5.70, and 5.72 are accumulated on an anisotropic lattice 8^4, $\gamma=2$, using the pseudo-heat-bath method. It is noted that the deconfining transition occurs at $\beta=5.67$ on this lattice.[12] The Polyakov line is measured for each configuration before cooling. In Fig. 1 scatter plots in terms of $\tilde{S}$ (normalized action) versus Q (topological charge) and I_Q versus Q at 100, 200, and 300 cooling stages for $\beta=5.64$ are shown. These plots show the approximate quantization of these quantities as cooling goes on. The units of quantization are 0.8–0.9 for Q and I_Q and ~ 1 for the normalized action. These values are similar to those observed on isotropic lattices. The convergence of the topological charge to quantized values is faster than that of the action. For the assignment of the topological charge and instanton number to each configuration we need more careful tracing of the cooling history and a semilocal study. One of the reasons is the decay or pair annihilation of the topological charge. In Fig. 2 several examples of cooling histories are shown. Configurations having a unit topological charge and unit normalized action are typically observed. An instanton event is shown in Fig. 2(a). In this example, semilocal distributions of Q, the electric action, and magnetic action show a clear localization and approximate self-duality, which is expected from an instanton nature [see Fig. 2(b)]. Sometimes the decay of the topological charge occurs before the convergence of the action, as shown in Fig. 2(c). However, the plateau of I_Q and the fact that semilocal distributions of Q show isolated localization [Fig. 2(d)] indicate this example is an instanton–anti-instanton pair. In this way, we can assign Q and I_Q except for a small number of configurations (less than 5%).

Most configurations are interpreted as those composed of instantons and anti-instantons. However, there are some configurations which cannot be interpreted as instanton type. One such group is seen in the configurations with vanishing Q and I_Q. In Fig. 3 scatter plots with respect to space-time action versus space-space action at the cooling stages of 100 (a), 200 (b), and 300 (c) for $Q=0$ and $I_Q=0$ events are presented. Although most configurations lose both the magnetic and electric action at the stage of 200 cooling, roughly 10% of them keep a sizable magnetic action greater than 0.3 at the 300 cooling stage. Such types of configuration are more often observed in the deconfinement phase rather than in the confinement phase. Analyses of these magnetic configurations will be presented in Sec. IV. Another class of configurations which does not belong to the instanton type also has been seen. In Fig. 4 an example of the cooling history and semilocal distributions of such configurations is presented. Although the normalized action and I_Q tend to converge to unit values, the topological charge vanishes. In the semilocal distributions, roughly half a unit of positive and negative topological charges localize. A remarkable fact is that such configurations are found in the confinement phase in the present sample. It seems quite interesting to investigate the interpretation of such configurations as meron–anti-meron pair. At present, however, because of limitation of the data sample, further investigation is not adequate.

B. Distribution of topological charge

Distributions of the topological charge Q and I_Q at different temperatures are displayed in Fig. 5. As shown in the figure, the distributions are narrower in high-temperature deconfining phases ($\beta=5.70,5.72$) than in low-temperature confining phases ($\beta=56.2,5.64$). As the range of β is limited to a neighborhood of β_c, such a suppression can hardly be explained by a trivial decreasing toward a larger β. To see this more clearly, we divide configurations at the same temperature ($\beta=5.70$) with respect to the value of the Polyakov line (less and greater

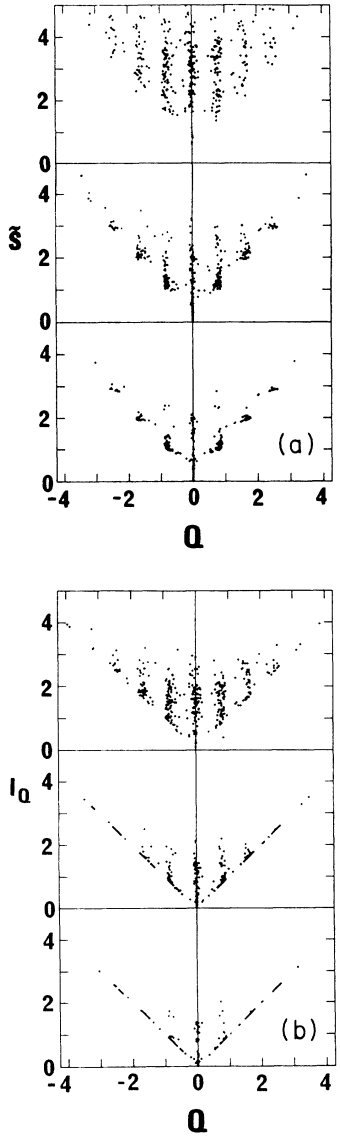

FIG. 1. (a) Scatter plots $\tilde{S}$ vs Q and (b) I_Q vs Q after 100 (top), 200 (center), and 300 (bottom) cooling sweeps. 8^4, $\gamma=2$ lattice at $\beta=5.64$ is used. Number of events is 400.

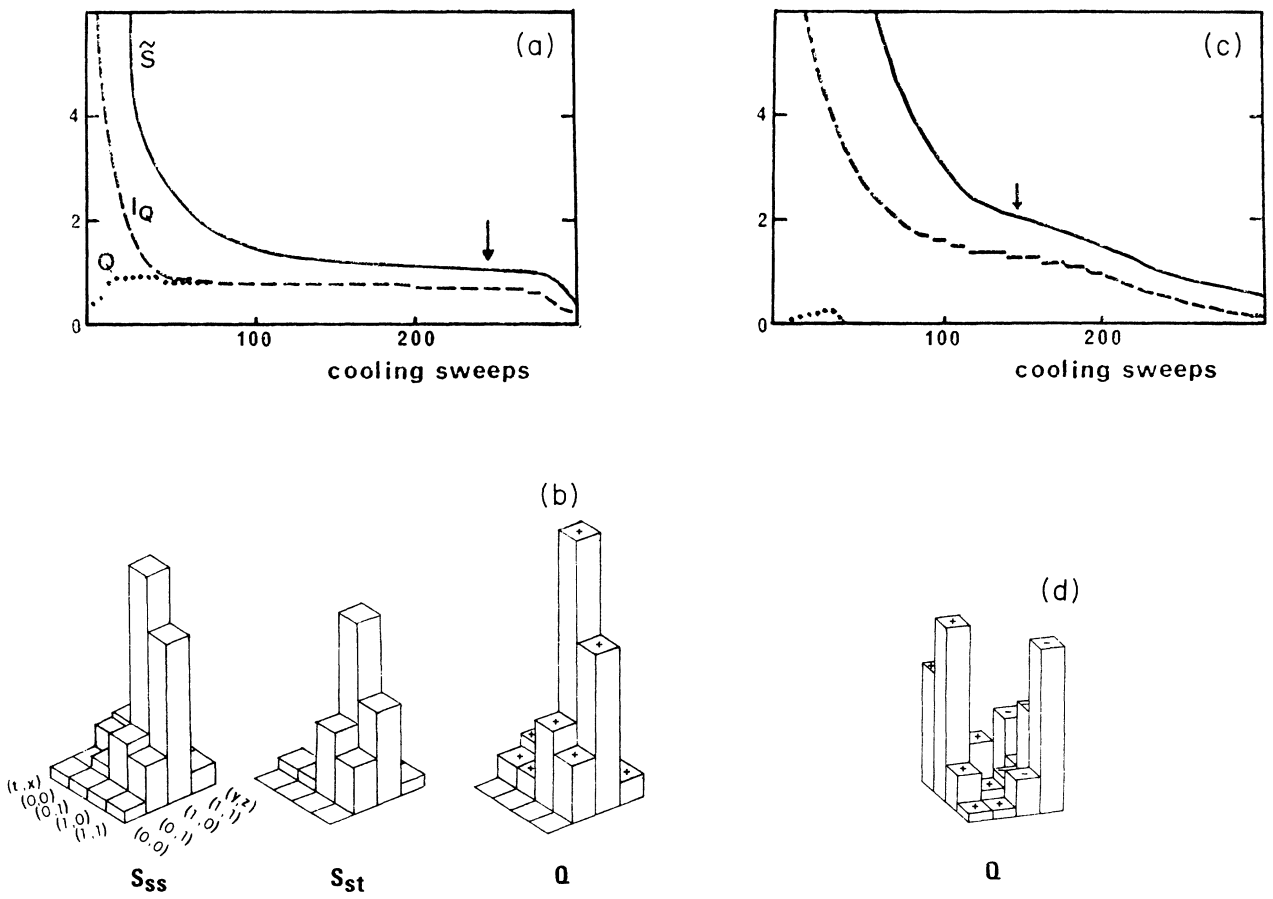

FIG. 2. Typical examples of cooling curves of $\tilde{S}$ (solid line), Q (dotted line), and I_Q (dashed line) (a) for a one-instanton configuration and (b) distribution of space-space (magnetic) action over 16 sublattices at the cooling stage represented (a) by the arrow. Similar distributions of space-time (electric) action and topological charge Q, (c) for a multi-instanton configuration with decay and (d) distribution of Q at the cooling stage represented (c) by the arrow.

than 0.1) to distinguish the confining phase from the deconfining one (Fig. 6). The resultant distribution for the confining group is prominently wider than that of the deconfining group although statistics is rather poor. Thus, suppressions of the topological charge and I_Q which is considered as the instanton density are observed in the present anisotropic lattice. Another feature is that, for $\beta=5.64$, the distribution seems to be narrower than Poissonian (dashed histogram). However we cannot take this point seriously because of the finite-size effect.

In Fig. 7 the average values of Q^2 and I_Q are presented. We obtained quite small values for both quantities above the critical point. Again, if we divide configurations with respect to the value of the Polyakov line to distinguish two phases, a suppression of Q^2 and I_Q in the deconfining phase becomes clear. Furthermore discontinuous types of behavior are observed. It is noted that the average value of the Polyakov line of the deconfining phase at $\beta=5.70$ is 0.195 in the present anisotropic lattice.

As for the topological susceptibility, the ratio with respect to the temperature near the critical point is given to be

$$\begin{aligned}\chi_t/T^4 &= \{\langle Q^2\rangle/[(a_sN_s)^3a_tN_t]\}/T^4 \\ &= \{\langle Q^2\rangle/[(a_sN_s)/(a_tN_t)]^3\} \\ &= \begin{cases} 0.156\pm0.008 & \text{for } \beta=5.64\ , \\ 0.0436\pm0.002 & \text{for } \beta=5.70\ , \end{cases} \end{aligned} \tag{8}$$

where the value of $a_s/a_t\simeq 2.6$ for $\gamma=2$ obtained in Ref. 12 is used. Similarly the instanton density n_Q is estimated to be

$$\begin{aligned} n_Q/T^4 &= \langle I_Q\rangle/[(a_sN_s)/(a_tN_t)]^3 \\ &= \begin{cases} 0.0978\pm0.005 & \text{for } \beta=5.64\ , \\ 0.0414\pm0.002 & \text{for } \beta=5.70\ . \end{cases} \end{aligned} \tag{9}$$

These values at $\beta=5.64$ give $\chi_t\simeq(144\ \text{MeV})^4$ and $n_Q\simeq(128\ \text{MeV})^4$ if we set $T=230$ MeV.

Suppressions of the topological charge and instanton density are observed in both the present anisotropic lattice and isotropic lattice.[7] Thus the suppression of the topological charge in the deconfining phase seems a dynamical issue related to the deconfining transition rather than a simple spilling out of the instanton from a coarse lattice.

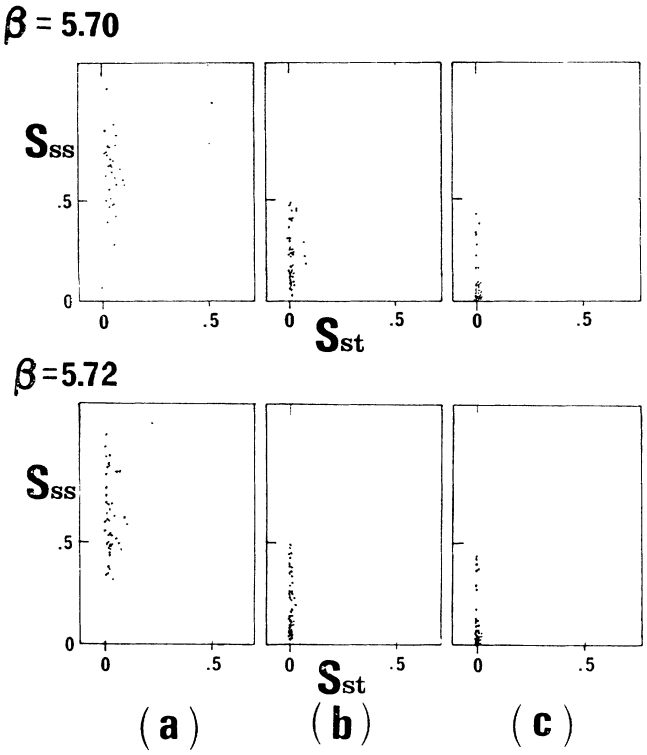

FIG. 3. Scatter plots with respect to a space-time action $\tilde{S}_{st}$ vs space-space action $\tilde{S}_{ss}$ for 50 $I_Q=0$ events after (a) 100 cooling sweeps, (b) 200 sweeps, and (c) 300 sweeps. (Time step $\delta=0.04$.)

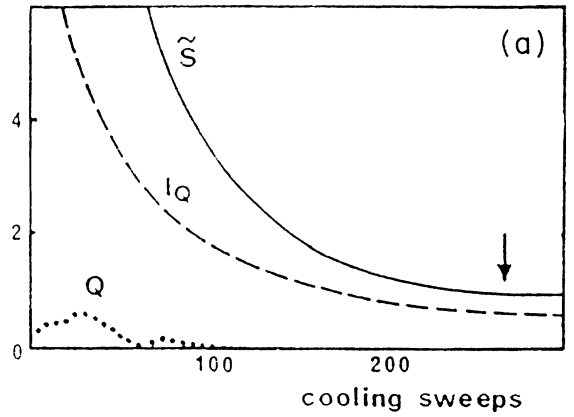

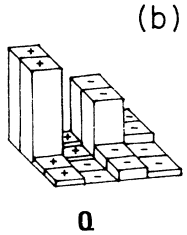

FIG. 4. Cooling curve of (a) a meron and (b) a semilocal distribution of Q.

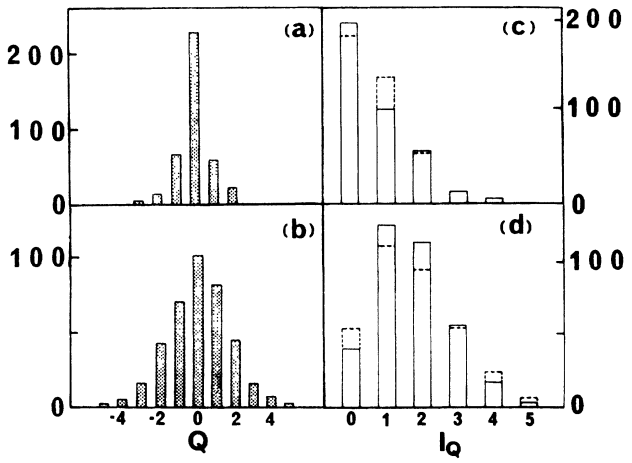

FIG. 5. Distributions of Q for (a) $\beta=5.70$ (b) $\beta=5.64$, and distributions of I_Q for (c) $\beta=5.70$, (d) $\beta=5.64$. Dashed lines represent Poisson distributions.

IV. ANALYSES OF MAGNETIC CONFIGURATIONS

Here we concentrate on the magnetic configurations which appear in the cooling analyses. As mentioned in Sec. III A a class of configurations in the sample of $Q=0$ and $I_Q=0$ (i.e., no instanton and anti-instanton) group have the following characteristics: (1) Space-space action shows a plateaulike behavior around 0.5–0.3 (in $4\pi^2\beta/3$ units) as cooling goes on; (2) for those configurations, the space-time action vanishes in the early stage of cooling; (3) distribution of the magnetic action is constant in a temporal direction.

On the present anisotropic SU(3) lattice (8^4, $\gamma=2$), we have about 200 configurations of $I_Q=0$ in the total 400 configurations. In these configurations, roughly 5–10% of them have the above characteristics at $\beta=5.70$–5.72 (note that $\beta_c=5.67$). For later convenience, we call such a configuration an M-type event. On the other hand, the configuration which loses the magnetic action as well as the electric one quickly is called a T-type event. Although such configurations have been observed and analyzed above and below the critical point in both SU(3)

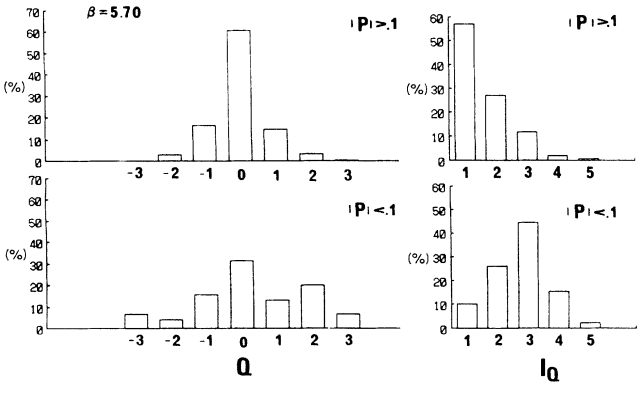

FIG. 6. Distributions of Q and I_Q at $\beta=5.70$ for deconfining ($|P|>0.1$) and confining ($|P|<0.1$) configurations.

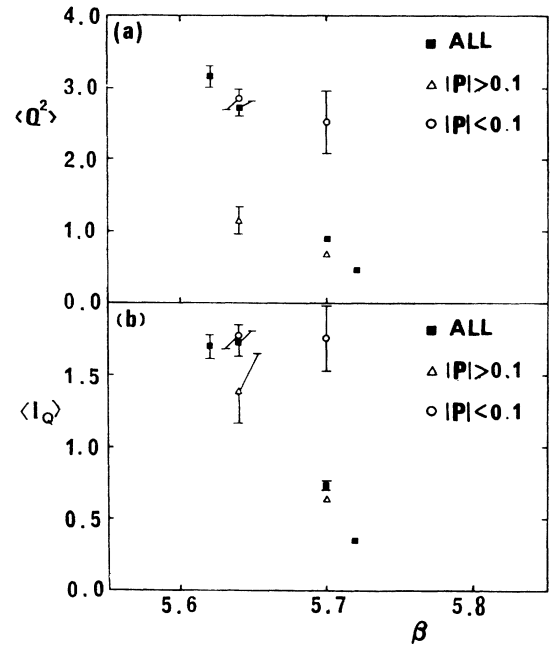

FIG. 7. Averages of (a) Q^2 and (b) I_Q above and below the critical point of the deconfining transition. Black squares correspond to the average over all configurations. Open triangles and open circles are the average over configurations having the values of the Polyakov line greater and smaller than 0.1, respectively.

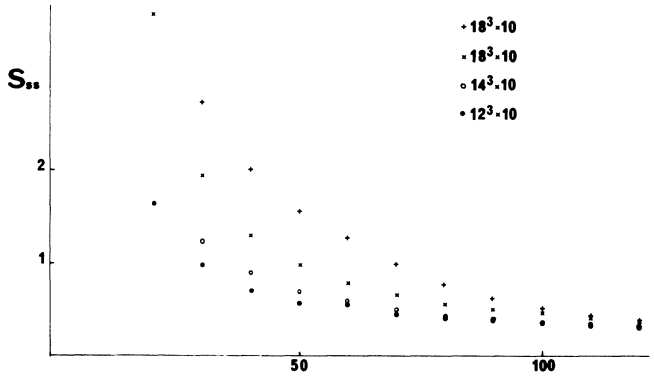

FIG. 8. Magnetic actions (S_{ss}) of typical SU(2) M-type events vs cooling sweeps for different lattice sizes and different boundary conditions. ×, ○, and ● are periodic boundary conditions and + is antiperiodic boundary conditions. Cooling sweeps are rescaled to sweep $\times 12/N_s$.

and SU(2) lattices, here we restrict ourselves in the deconfinement region. An obvious question on the appearance of such a cooling pattern is whether it depends on the method of cooling. On this problem, we have made supplemental studies on both isotropic and anisotropic SU(2) lattices. Comparisons are made for (a) results of heat-bath cooling with an infinite β and cooling by the equation of motion for the same SU(2) configuration and (b) cooling curves of different time steps ($\delta=0.008,0.02,0.08$) for the same SU(2) configuration. As shown in Table I, we see roughly the same plateaulike behavior if we suitably rescale the cooling steps. The dependence on the path of cooling in a sweep has been also checked and no substantial differences have been observed. Thus the appearance of such magnetic behavior is insensitive to the details of the cooling method.

The dependence on the size of the lattice is important from the viewpoint of the finite-size effect. To see this we need further extensive investigation in larger lattices. In the present stage, we have found such magnetic configurations in SU(2) lattices with a size up to 10×20^3 for both periodic and antiperiodic space boundary conditions. In Fig. 8 typical examples of plateaulike behavior in the cooling process in an SU(2) lattice of $10\times 12^3, 14^3, 18^3$ (periodic and anti-periodic boundary conditions) in the deconfinement region are shown. In these examples, there is no substantial difference in the plateau behavior and its height.

A. Magnetic field and charge

In this section, the results of magnetic charge measurements for M-type configurations defined in the previous section are reported. An interesting possibility for the M-type configuration is the one with a magnetic monopole. Although a magnetic monopole in a non-Abelian gauge system does not exist in the classical level, the possible existence under a quantum-induced adjoint scalar field has been pointed out.[4] Analyses from this point of

TABLE I. Comparisons of the cooling history of the space-space action between the Langevin with $\delta=0.04$ and heat-bath methods (a), and between different time steps ($\delta=0.02,0.01,0.002$) in the Langevin method (b).

			(a)			
	Cooling sweep	S_{ss}	Cooling sweep	S_{ss}	Cooling sweep	S_{ss}
$\delta=0.04$	15	4.7	45	1.89	300	0.45
Heat bath	5	4.7	15	1.69	100	0.44
			(b)			
δ						
0.02	10	19.7	20	7.25	40	3.25
0.01	20	21.1	40	7.20	80	3.42
0.002	100	22.6	200	7.05	400	3.38

view for such configurations in an SU(2) lattice have been reported in Ref. 10 and the results support the view. In the case of the SU(3) lattice, enough analysis has not been made yet. Furthermore, the possibility that such magnetic behavior is produced by cooling from a class of instanton configurations, has been pointed out recently.[14] Motivated by these facts, we have analyzed the magnetic field of an M-type configuration in our SU(3) lattice along with cooling. Here, magnetic fields are measured for these events based on a U(1) projection to the Polyakov line P (unitary gauge) because it is an ordered field at least in the deconfining region. Namely, $\ln(P)/i$ is considered a Higgs field.[4] Following the procedure in Ref. 8, Abelian magnetic fields are extracted. In the first step, eigenvalues of $\ln(P)$ are evaluated at each site and three eigenvalues are rearranged in the decreasing order to obtain a smooth "Higgs field" over the lattice. Then, the U(1) field defined on a link $U_\alpha(n)$ with respect to an eigenspace of an ith eigenvalue of $\ln(P)$ $(i=1,2,3)$ is defined as

$$\theta_\alpha^{(i)}(n)=\mathrm{Arg}\langle n,(i)|U_\alpha(n)|n+\alpha,(i)\rangle \ , \tag{10}$$

where $|n,(i)\rangle$ is an eigenvector belonging to the ith eigenvalue of $\ln(P)$ at site n. The corresponding U(1) field strength associated with a plaquette $P_{\alpha\beta}$ is

$$F_{\alpha\beta}^{(i)}(n)=\mathrm{mod}[\theta_\alpha^{(i)}(n)+\theta_\beta^{(i)}(n+\alpha)-\theta_\alpha^{(i)}(n+\beta) -\theta_\beta^{(i)}(n),2\pi] \ . \tag{11}$$

The magnetic charge of a space cube(n) corresponding to the Abelian field (11) is

$$Q_m^{(i)}(n)=\sum_{r\in\mathrm{cube}(n)} F_{\alpha\beta}^{(i)}(r) \ . \tag{12}$$

We have applied this procedure to about ten SU(3) M-type configurations. In Fig. 9 the magnetic charge and flux distributions (at a time slice) of two M-type configurations at several cooling stages are shown. In the early stage of cooling, many magnetic charges and anticharges are seen and those distributions vary time slice to time slice. As cooling goes on further, a nontrivial three-dimensional magnetic structure appears. In most cases, a few pairs of magnetic charge remain, as shown in Fig. 9(a). In some cases, no magnetic charges are found but a kind of squeezed magnetic flux is left, as shown in Fig. 9(b). Sometimes, magnetic charge pairs are created at the position of squeezed flux by further cooling. For T-type configurations, no such magnetic structure has been seen in the deep cooling stage. Correlations between these magnetic structures and the Polyakov line have been seen in the following analyses. In Fig. 10, for an M-type configuration, we display the spatial distribution of the magnetic action 10(a), the largest eigenvalue of $\ln(P)/i$ 10(b), the magnetic charge 10(c), and the sum of the absolute square of an off-diagonal element of space link (x direction in this example) 10(d), which is defined as

$$\tfrac{1}{3}\sum_{i,j=1,\,i\neq j}^{3}|\langle n,(i)|U_x(n)|n+x,(j)\rangle|^2 \ , \tag{13}$$

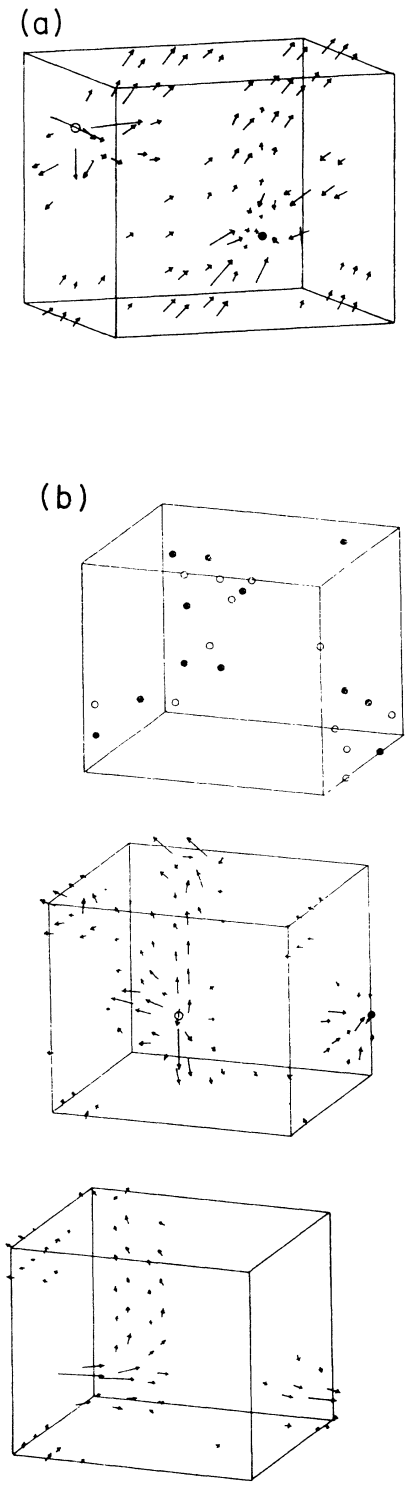

FIG. 9. (a) An example of magnetic flux, charge (○) and anticharge (●) of an M-type configuration [$i=1$ eigenstate in Eqs. (10)–(12)] (after 400 cooling sweeps with time step $\delta=0.08$). (b) Top, magnetic charge of an M-type configuration ($i=1$) after ten cooling sweeps. The magnetic flux is omitted in the figure. Middle, magnetic flux and charge of the same configuration as top figure after 100 cooling sweeps. Bottom, similar to middle figure except for 200 cooling sweeps. The squeezed flux is left although no charge is seen.

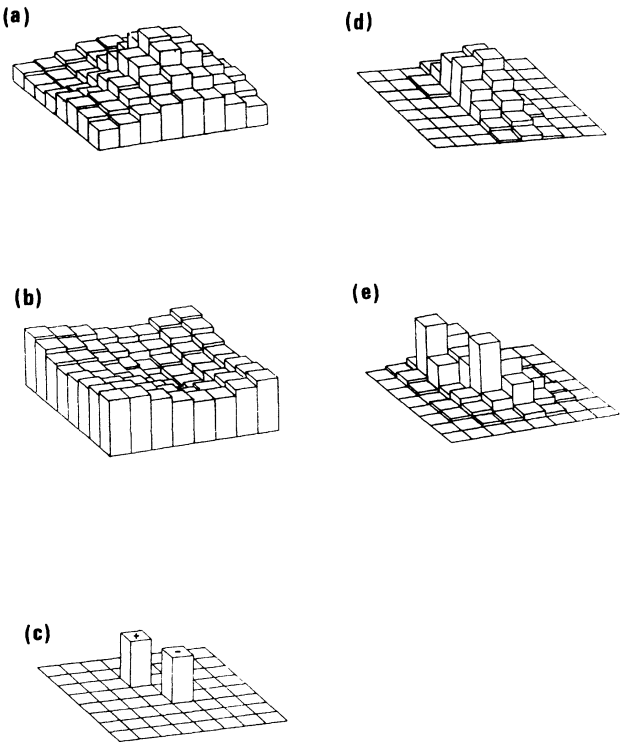

FIG. 10. (a) Spatial distributions of the magnetic action, (b) the largest eigenvalue of $\ln P$, (c) the magnetic charge, (d) the strength of off-diagonal element squared of the space link, and (e) the strength of magnetic flux of an M-type event ($i=1$ and two-dimensional section including monopole and antimonopole).

and tells us about the strength of the color rotation around the site n. The strength of the magnetic flux is shown in Fig. 10(e). A remarkable point is that most space links are approximately diagonalized simultaneously with the Polyakov line except for in the neighborhood of the magnetic charge. The dip of the eigenvalue of $\ln(P)$ and the position of charge is consistent with the SU(2) case in Ref. 10. These features are consistent with the semiclassical monopole in the gauge $-\ln(P)/i$ is a Higgs field. However, some points are left unsolved. As seen in Fig. 10(a), the distributions of the magnetic action spread over widely more than other quantities, and have a nonvanishing value even where the charge and flux vanish. Therefore, the relation between the mechanism for sustaining the magnetic action and the existence of a monopole may not be as simple as in the semiclassical monopole picture. Another point is that creation and annihilation of a close pair of magnetic charges are easily induced by a small quantum effect. For example, if we add small Gaussian random noise of the 10^{-3} level to the right-hand side of Eq. (2), many pairs of magnetic charge appear. However, if we switch off the noise and return to normal cooling, we see a few monopole pairs or a squeezed magnetic flux again. Thus, the short-range structure might receive a cooling artifact. On the other hand, a middle- or long-range magnetic structure looks free of the cooling artifact. For example, charges and flux at 10, 100, and 200 cooling sweeps, shown in Fig. 9(b) distribute over a common region although the number of charges changes. This feature seems different from recent observations of the magnetic monopole and Dirac string in the three-dimensional George-Glashow model.[15]

As for the stability of the presently observed squeezed flux structure, studying of the finite-size effect seems quite important. About this point, as mentioned before, we have observed an M-type configuration in an SU(2) lattice up to 10×20^3 with both periodic and antiperiodic boundary conditions. These magnetic features are found irrespective of the lattice size and space boundary condition.

B. Three-dimensional fermionic zero mode

One characteristic of M-type configurations in the deep cooling stage is its three-dimensional (i.e., static) structure.[16] In the previous section, a charge or squeezed magnetic flux is found. Although the existence of a magnetic structure certainly is seen, some portion might depend on the cooling. In this section, we further study M-type configurations from the viewpoint of the zero mode in a three-dimensional fermionic (Dirac) operator. In the studies of the instanton, the existence of zero modes in a four-dimensional fermionic operator have been reported.[17]

The fermion operator adopted here is the three-dimensional staggered fermion[14] operator

$$D_{mn}=i\frac{\eta_\alpha(n)}{2}[U_\alpha(n)\delta_{m,n+\alpha}-U_\alpha^\dagger(n-\alpha)\delta_{m,n-\alpha}]\ , \quad (14)$$

where

$$\eta_\alpha(n)=(-1)^{n_1+n_2+\cdots+n_{\alpha-1}}\ . \quad (15)$$

The eigenvalue of this operator are analyzed by using Lanczos and Householder transformation methods. We apply the analysis for three-dimensional configurations changing time slices. In Fig. 11 distributions of the eigenvalue squared of typical M- and T-type configurations up to initial 10 cooling are shown. For T-type events, all levels go upward as cooling goes on and there is no small eigenvalue corresponding to the zero mode. On the other hand, for M-type configurations, a few lowest levels remain small whereas higher levels shift upward with cooling. They are an order of magnitude smaller in comparison with the other level. Such a pattern of eigenvalues is commonly seen at every time slice. Thus, these levels with small eigenvalues are identified as the three-dimensional zero mode.

Such small eigenvalues are also found in configurations having a squeezed magnetic flux, as shown in Fig. 9(b). We also note that the existence of zero modes seems stable against small perturbations, as stated in Sec. IV B. A similar analysis is applied to configurations having an instanton. In this case, the existence of small eigenvalues depends on the time slice, as expected from the four-dimensional nature of the instanton. Thus, based on these analysis, the existence of such a three-dimensional

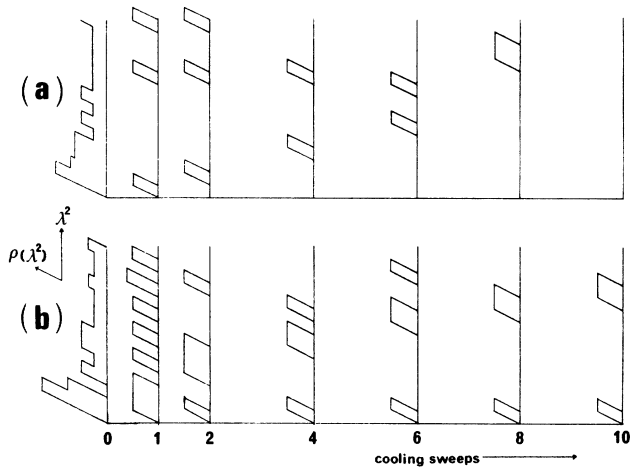

FIG. 11. Distribution of a few smallest eigenvalues squared and its density for (a) a T-type event and (b) an M-type event vs cooling. Separation of the smallest eigenvalue (b) is evident.

zero mode irrespective of time slices seems a good characteristic of M-type configurations. The distinction of M-type configurations from those of instanton type is rather clear in this way.[14]

V. SUMMARY AND DISCUSSION

The topological properties of the SU(3) gauge field on an anisotropic lattice (8^4, $a_s/a_t \approx 2.6$) near the critical temperature are studied. Semilocal measurements of the topological charge, the sum of the absolute value of the topological charge density I_Q, and the electric action and magnetic action are used to classify configurations in the framework of the cooling method. Most configurations are consistent with those composed of instantons and antiinstantons. The distribution of the topological charge and I_Q in the deconfining phase is drastically suppressed in comparison with those in the confinement phase. Some other classes which cannot be interpreted as instanton type are also found.

A class of configurations which have a plateau in the magnetic action and a vanishing topological charge density in the cooling stage is studied in detail. The appearance of the plateau seems insensitive to the cooling methods. In an SU(2) lattice, such a class of configurations is found in a 10^4 (anisotropy=2) to 10×20^3 lattice. In the case of an 8^4 (anisotropy parameter equal to) SU(3) lattice, the rate of such configurations is about 5–10 % of the total $I_Q=0$ events, slightly above the critical point ($\beta=5.70$–5.72). The magnetic charge in a unitary gauge and the three-dimensional fermionic zero mode are examined along with cooling. A few pairs of isolated magnetic charges or squeezed magnetic flux are found in the deep region of cooling. Most space links are simultaneously diagonalized with the Polyakov line, except in the neighborhood of the magnetic charge. A dip structure of the eigenvalue of the logarithm of the Polyakov line is found near the position of the magnetic charge. As for eigenvalues of the three-dimensional staggered fermion operator, a few lowest eigenvalues keep their smallness in contrast with the upward shift of higher levels in cooling. This separation can be seen rather quickly after the start of cooling sweeps. This seems a good characteristic of M-type configurations. Most of the above results suggest that M-type configurations in the deep cooling stage include a monopole consistent with the semiclassical picture or a certain squeezed magnetic flux. Many points are still unsolved in this picture. For examples, the relation between the distribution of the action and the magnetic field and details of the squeezed flux should be analyzed. Another important question is the use of cooling in a magnetic field analysis. On this problem, some results, such as the identification of the zero mode, or a relevant region of the magnetic structure as discussed in Sec. IV B, are established soon after cooling.

An anisotropic lattice provides a good resolution to describe the temporal structure even at high temperatures, in contrast with the ordinary isotropic lattice. In this sense, the observations of the dual structure of instantons and the static nature of the magnetic configurations in Sec. IV (no structure in temporal direction) seem remarkable.

ACKNOWLEDGMENTS

The authors would like to thank Dr. F. Karsch, Dr. A. Nakamura, and Dr. I. O. Stamatescu for discussions and communications about the anisotropic lattice. They thank also Dr. C. DeTar for discussion, encouragement, and reading the manuscript. They also thank Dr. M. L. Laursen for a notice on the Dirac sheet. The authors acknowledge the RADIUS-Co. for technical support in computation. The numerical simulations of the present work were performed using the computers NEC SX-2N at the Computer Center of Osaka University and NEC SX-2 at the NEC Fundamental Research Laboratory.

[1]G. 't Hooft, Phys. Rev. Lett. **37**, 3432 (1976).
[2]C. Callan, R. Dashen, and D. Gross, Phys. Rev. D **17**, 2717 (1978).
[3]E. Witten, Nucl. Phys. **B156**, 269 (1979); G. Veneziano, *ibid.* **B159**, 213 (1979).
[4]G. 't Hooft, in *High Energy Physics*, edited by A. Zichichi (Editorice Compositori, Bologna, 1976); Nucl. Phys. **B190**, 455 (1980); Phys. Scr. **25**, 133 (1982); S. Mandelstam, Phys. Rep. **23C**, 245 (1976).
[5]J. Polonyi, Phys. Lett. B **213**, 340 (1988).
[6]B. Berg, Phys. Lett. **104B**, 475 (1981); Y. Iwasaki and T. Yoshie, *ibid.* **125B**, 197 (1983); **131B**, 159 (1983); J. Hoek, M. Teper, and J. Waterhouse, Phys. Lett. B **180**, 112 (1986); Nucl. Phys. **B288**, 589 (1987); J. Hoek, Phys. Lett. **166B**, 199 (1986).
[7]M. Teper, Phys. Lett. **162B**, 357 (1985); Phys. Lett B **171**, 81

(1986); **171**, 86 (1986); **202**, 553 (1988); **206**, 299 (1988); E. M. Ilgenfritz, M. L. Laursen, M. Müller-Preussker, G. Schierholz, and H. Schiller, Nucl. Phys. **B268**, 693 (1986); M. I. Polikarpov and A. I. Veselov, *ibid.* **B297**, 34 (1988).

[8]J. Polonyi, Nucl. Phys. **A461**, 279c (1987).

[9]A. S. Kronfeld, M. L. Laursen, G. Schierholz, and U. J. Wiese, Phys. Lett. B **198**, 516 (1988).

[10]M. L. Laursen and G. Schierholz, Z. Phys. C **38**, 501 (1988).

[11]J. Kuti, J. Polonyi, and K. Szlachanyi, Phys. Lett. **98B**, 199 (1981); S. Das and J. B. Kogut, *ibid.* **145B**, 375 (1984); Nucl. Phys. **B265**, 303 (1986); J. C. Sexton and H. B. Thacker, Phys. Rev. Lett. **57**, 2131 (1986).

[12]G. Burgers, F. Karsch, A. Nakamura, and I. O. Stamatescu, Nucl. Phys. **B304**, 587 (1988).

[13]A. Guha and S. C. Lee, Phys. Rev. D **27**, 2412 (1983); S. Grunewald, E. M. Ilgenfritz, and M. Müller-Preussker, Z. Phys. C **33**, 561 (1987).

[14]S. Hands, Nucl. Phys. **B329**, 205 (1990).

[15]M. L. Laursen and M. Müller-Preussker, Nucl. Phys. **B313**, 1 (1989).

[16]G. 't Hooft, Nucl. Phys. **B109**, 455 (1981); A. Sinha, Phys. Rev. D **14**, 2016 (1976).

[17]P. Woit, Phys. Rev. Lett. **51**, 638 (1982); Nucl. Phys. **B262**, 284 (1985); Y. Arian and P. Woit, Phys. Lett. **169B**, 402 (1986); Nucl. Phys. **B268**, 521 (1986); M. Luscher, Commun. Math. Phys. **85**, 29 (1982); I. A. Fox, J. P. Gilchrist, M. L. Laursen, and G. Schierholz, Phys. Rev. Lett. **54**, 749 (1985).

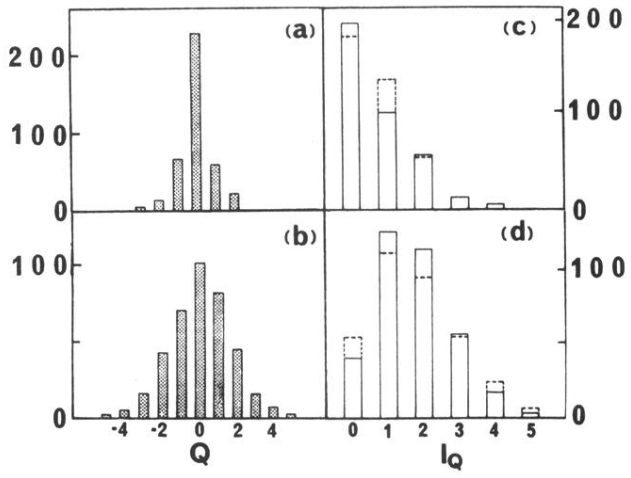

FIG. 5. Distributions of Q for (a) $\beta=5.70$ (b) $\beta=5.64$, and distributions of I_Q for (c) $\beta=5.70$, (d) $\beta=5.64$. Dashed lines represent Poisson distributions.